

# In Situ Observation of Low-Power Nano-Synaptic Response in Graphene Oxide Using Conductive Atomic Force Microscopy

Fei Hui,\* Peisong Liu, Stephen A. Hodge, Tian Carey, Chao Wen, Felice Torrissi, D. Thanuja L. Galhena, Flavia Tomarchio, Yue Lin, Enrique Moreno, Juan B. Roldan, Elad Koren, Andrea C. Ferrari, and Mario Lanza\*

Multiple studies have reported the observation of electro-synaptic response in different metal/insulator/metal devices. However, most of them analyzed large ( $>1 \mu\text{m}^2$ ) devices that do not meet the integration density required by industry ( $10^{10}$  devices/ $\text{mm}^2$ ). Some studies employed a scanning tunneling microscope (STM) to explore nano-synaptic response in different materials, but in this setup there is a nanogap between the insulator and one of the metallic electrodes (i.e., the STM tip), not present in real devices. Here, it is demonstrated how to use conductive atomic force microscopy to explore the presence and quality of nano-synaptic response in confined areas  $<50 \text{ nm}^2$ . Graphene oxide (GO) is selected due to its easy fabrication. Metal/GO/metal nano-synapses exhibit potentiation and paired pulse facilitation with low write current levels  $<1 \mu\text{A}$  (i.e., power consumption  $\approx 3 \mu\text{W}$ ), controllable excitatory post-synaptic currents, and long-term potentiation and depression. The results provide a new method to explore nano-synaptic plasticity at the nanoscale, and point to GO as an important candidate for the fabrication of ultrasmall ( $<50 \text{ nm}^2$ ) electronic synapses fulfilling the integration density requirements of neuromorphic systems.

the adjustment of their electrical resistance depending on the history of electrical stresses applied.<sup>[1]</sup> Depending on the materials employed, MIM devices can exhibit: i) two stable resistive states (often called non-volatile RS), used to fabricate binary electronic memories;<sup>[2]</sup> and ii) one stable and one unstable resistive state (often called threshold RS), explored for the fabrication of electronic neurons, i.e., devices for signal integration and electrical spike generation in artificial neural networks (ANNs);<sup>[3]</sup> and iii) multiple stable resistive states (often called analogue RS), explored for the fabrication of electronic synapses, i.e., devices that define the strength of the connection between electronic neurons in ANNs.<sup>[3]</sup> The fabrication of state-of-the-art electronic memories and ANNs using MIM-like RS devices requires high integration density ( $>10^{10}$  devices/ $\text{mm}^2$ ),<sup>[4]</sup> i.e. the RS must be demonstrated in ultras-small devices ( $<100 \text{ nm}^2$ ).<sup>[5-7]</sup> The smallest

memristors fabricated to date have sizes  $\approx 2 \text{ nm} \times 2 \text{ nm}$  and a Pt/TiO<sub>2</sub>/HfO<sub>2</sub>/Pt structure,<sup>[6]</sup> but just few RS cycles were demonstrated and the switching voltages presented a high variability ( $>2 \text{ V}$ ). Ref. [7] presented a complete statistical analysis in

## 1. Introduction

Resistive switching (RS) is a phenomenon occurring in different metal/insulator/metal (MIM) devices that consists on

Dr. F. Hui, Prof. E. Koren  
Department of Materials Science and Engineering  
Technion – Israel Institute of Technology  
Haifa 3200003, Israel  
E-mail: fei.hui@campus.technion.ac.il

Dr. P. Liu, C. Wen  
Institute of Functional Nano & Soft Materials  
Collaborative Innovation Center of Suzhou Nanoscience and Technology  
Soochow University  
199 Ren-Ai Road, Suzhou 215123, China

Dr. S. A. Hodge, Dr. T. Carey,<sup>[†]</sup> Dr. F. Torrissi,<sup>[†]</sup> Dr. D. T. L. Galhena,  
Dr. F. Tomarchio, Dr. Y. Lin, Prof. A. C. Ferrari  
Cambridge Graphene Centre  
University of Cambridge  
9 JJ Thomson Avenue, Cambridge CB3 0FA, UK

 The ORCID identification number(s) for the author(s) of this article can be found under <https://doi.org/10.1002/smll.202101100>.

<sup>[†]</sup>Present address: Molecular Science Research Hub, Department of Chemistry, Imperial College London, 82 Wood Lane, London W12 0BZ, UK

Dr. E. Moreno  
UJM-Saint-Etienne  
CNRS  
Institute of Optics Graduate School  
University of Lyon  
Laboratoire Hubert Curien UMR5516, St-Etienne F-42023, France  
Prof. J. B. Roldan  
Departamento de Electrónica y Tecnología de Computadores  
Universidad de Granada  
Facultad de Ciencias, Avd. Fuentenueva s/n, Granada 18071, Spain  
Prof. M. Lanza  
Physical Science and Engineering Division  
King Abdullah University of Science and Technology (KAUST)  
Thuwal 23955-6900, Saudi Arabia  
E-mail: mario.lanza@kaust.edu.sa

DOI: 10.1002/smll.202101100

10 nm × 10 nm memristors in with TiN/Hf/HfO<sub>2</sub>/TiN structure. However, observing RS in small areas <100 nm<sup>2</sup> is challenging.

One approach to explore the presence of RS in a materials system is the use of scanning probe microscopy (SPM) techniques, as they allow to characterize multiple nano-sized MIM cells (with sizes ranging from 1<sup>[8]</sup>–50 nm<sup>[9]</sup>). SPM techniques like scanning tunneling microscopy (STM) and conductive atomic force microscopy (CAFM) have been often employed to study binary RS in different materials.<sup>[10,11]</sup> However, the use of SPM techniques to explore other types of RS (i.e., analogue, threshold) for the fabrication of electronic synapses and neurons is still incipient. Refs. [10,11] used the tip of a STM as a top electrode to analyze nanogap-based Ag<sub>2</sub>S and Cu<sub>2</sub>S atomic switches, and observed short term plasticity (STP, i.e., volatile changes in resistance that recover after few milliseconds or seconds)<sup>[12]</sup> and long term plasticity (LTP, i.e., non-volatile changes in resistance that remain stable for minutes or days).<sup>[13]</sup> However, in refs. [10,11] the STM probe did not physically contact the device surface. Therefore the electrical characteristics were affected by the nanogap between tip and sample, which can be very unstable and produce high point-to-point variability. On the contrary, CAFM provides physical and stable contact between tip and sample, as well as accurate control of the contact force ( $F_C$ ) between them,<sup>[14]</sup> and it is overall more suitable than STM to form nano-sized MIM contacts.

Here, we use CAFM to study the nano-synaptic response in graphene oxide (GO) films prepared by liquid phase exfoliation (LPE)<sup>[15]</sup> and deposited by spray coating on metal-varnished Si wafers. The CAFM Pt tip is connected to a Keysight B1500A semiconductor parameter analyzer (SPA), so that ramped voltage stresses (RVS) and sequences of pulsed voltage stresses (PVS) can be applied locally, and the current signal can be simultaneously measured in situ from ±1 pA to ±1 mA.<sup>[16,17]</sup> Our experiments indicate that nanosized (≈50 nm<sup>2</sup>) metal/GO/metal cells have different synaptic responses enabled by volatile RS, such as potentiation and paired pulse facilitation (PPF) at low current <1 μA, controllable excitatory post-synaptic current (EPSC), smooth potentiation and depression, and non-volatile bipolar RS, necessary to achieve reproducible LTP.

We use GO for multiple reasons. First, the materials employed in RS devices are mainly transition metal oxides (TMO), but there are difficulties in using them for analogue

and threshold RS. Therefore, new materials need to be explored<sup>[18–20]</sup>. GO has already shown non-binary RS<sup>[21–23]</sup> in large devices (areas > 7000 μm<sup>2</sup>). Second, GO can be prepared inexpensively via LPE. Spray-coating allows conformal coverage surfaces with complex shapes.<sup>[24]</sup> This approach is very attractive from an industrial point of view. And third, GO is a layered material with high flexibility and transparency.<sup>[25,26]</sup> Previous studies reported that GO-based devices exhibit multiple RS-related phenomena, including STP, LTP, spike-timing dependent plasticity (STDP) in modified GO-based transistors,<sup>[21]</sup> STP and PPF in Ag/N-GOQD/Pt (where N-GOQD stands for N-doped GO quantum dots)<sup>[22]</sup> and EPSC, and PPF in crossbar arrays made of yarn coated with GO.<sup>[23]</sup> However, the sizes of all GO-based memristive devices reported to date are large (>7000 μm<sup>2</sup>).<sup>[21–23]</sup> Electro-synaptic behaviors at the nanoscale are required for GO to be used in high-density ANNs (>10<sup>10</sup> devices/mm<sup>2</sup>). Here, we show that GO can exhibit multiple nano-synaptic electronic phenomena at the nanoscale, attractive for the fabrication of ultrascaled electronic synapses and neurons.

## 2. Results and Discussion

We prepare GO flakes by a wet chemical method as detailed in Experimental Section. Transmission electron microscopy (TEM) (Figure 1a) shows that these have areas >20 μm<sup>2</sup>. The GO flakes are then deposited on Au-varnished SiO<sub>2</sub> wafers using a spray-coater (see Experimental Section), which allows scalable fabrication of devices.<sup>[27]</sup> The GO thickness on the metal can be controlled by adjusting the pressure of the spray-coater and the spraying time. Figure 1b is a topographic atomic force microscopy (AFM) map of the surface of a GO/Au/SiO<sub>2</sub> wafer. The root mean square roughness of the flat regions (i.e., without wrinkles) is ≈2.75 nm, as extracted by processing the topographic AFM images offline, using the NanoScope Analysis AFM software. This is similar to that of GO films prepared by spin coating.<sup>[26]</sup> The ability of spray-coating to cover any complex surface is demonstrated using bulk Pt tips as substrate. Wettability measurements are used to confirm the existence of oxygen-containing functional groups and the hydrophilic nature of the flakes (see Figure S1a,b, Supporting Information).

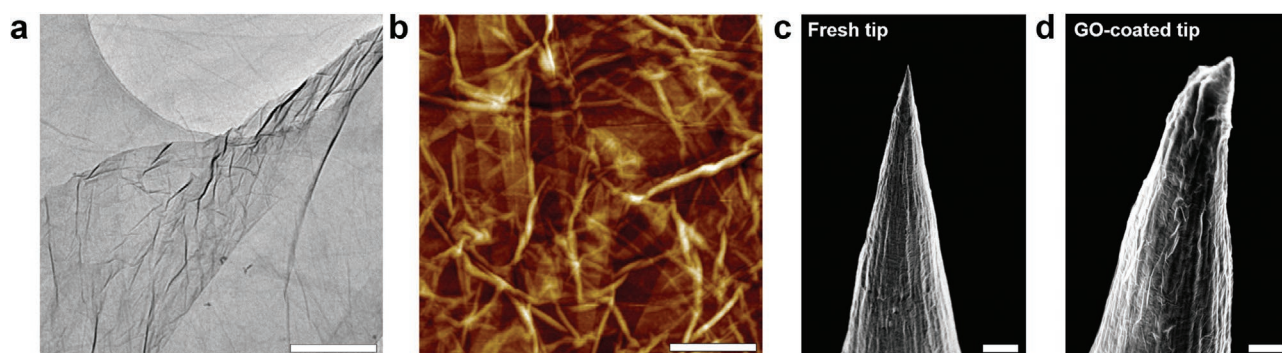


**Figure 1.** Morphological characterization of spray-coated GO. a) TEM image of GO flake. Scale bar = 500 nm. b) Topographic AFM map of a GO/Au/SiO<sub>2</sub> wafer. Scale bar = 500 nm. The color scale (Z-axis) is: black 0 nm, white 20 nm. c,d) SEM images of as-received Pt tip (without GO coating) and GO-coated Pt tip (after coating). Scale bars are 2.5 μm in (c) and 1 μm in (d).

Figures 1c,d are scanning electron microscopy (SEM) images of a pristine bulk Pt tip (without GO) and a GO-coated bulk Pt tip, respectively. These images show that conformal GO coating is achieved (as indicated by the formation of wrinkles). Similar results are found in other CAFM tips with different geometries (see Figure S1c, Supporting Information).

To construct nanosized GO-based memristive electronic synapses, we use two configurations. 1) A bulk Pt tip placed at a single location on the surface of a GO/Au/SiO<sub>2</sub> wafer, which leads to Pt/GO/Au nano-synapses with an effective area (between tip and sample) <math><50 \text{ nm}^2</math>,<sup>[9]</sup> given that the typical radius of the Pt tips is  $\approx 8 \text{ nm}$  (see Figure S2, Supporting Information). 2) A GO-coated bulk Pt tip placed on the surface of a Cu film, which leads to Pt/GO/Cu nano-synapses with slightly larger effective areas <math><500 \text{ nm}^2</math>, as the radius of the GO-coated tip is larger than that of the uncoated tip, due to the additional

thickness of the GO film ( $\approx 65 \text{ nm}$ , as demonstrated by close inspection of SEM images, see Figure S2, Supporting Information). Both types of structures are shown schematically in Figure 2. More details about the estimation of the effective size of the nano-synapses are in Note S1, Supporting Information.

Figure 2b plots the current versus voltage ( $I$ - $V$ ) curves collected on a single location of the Pt/GO/Cu nano-synapse in Figure 2a when exposed to a sequence of 20 RVS from 0 to 5 V across the Pt and Cu electrodes ( $V_{\text{TIP}}$ ), using a standard CAFM (see Figure 2d). During the forward  $I$ - $V$  curves (blue), only electrical noise is initially detected (at  $V_{\text{TIP}} < 1 \text{ V}$ ). At  $V_{\text{TIP}} \approx 1 \text{ V}$ , the currents start to increase progressively. At  $V_{\text{TIP}} \approx 3 \text{ V}$  the currents increase abruptly until reaching the saturation level of the CAFM ( $\pm 5 \text{ nA}$ ). The backward  $I$ - $V$  curves (dark yellow) show a current shift toward lower potentials, indicating that the resistivity of the Pt/GO/Cu nano-synapse has decreased. The fact that

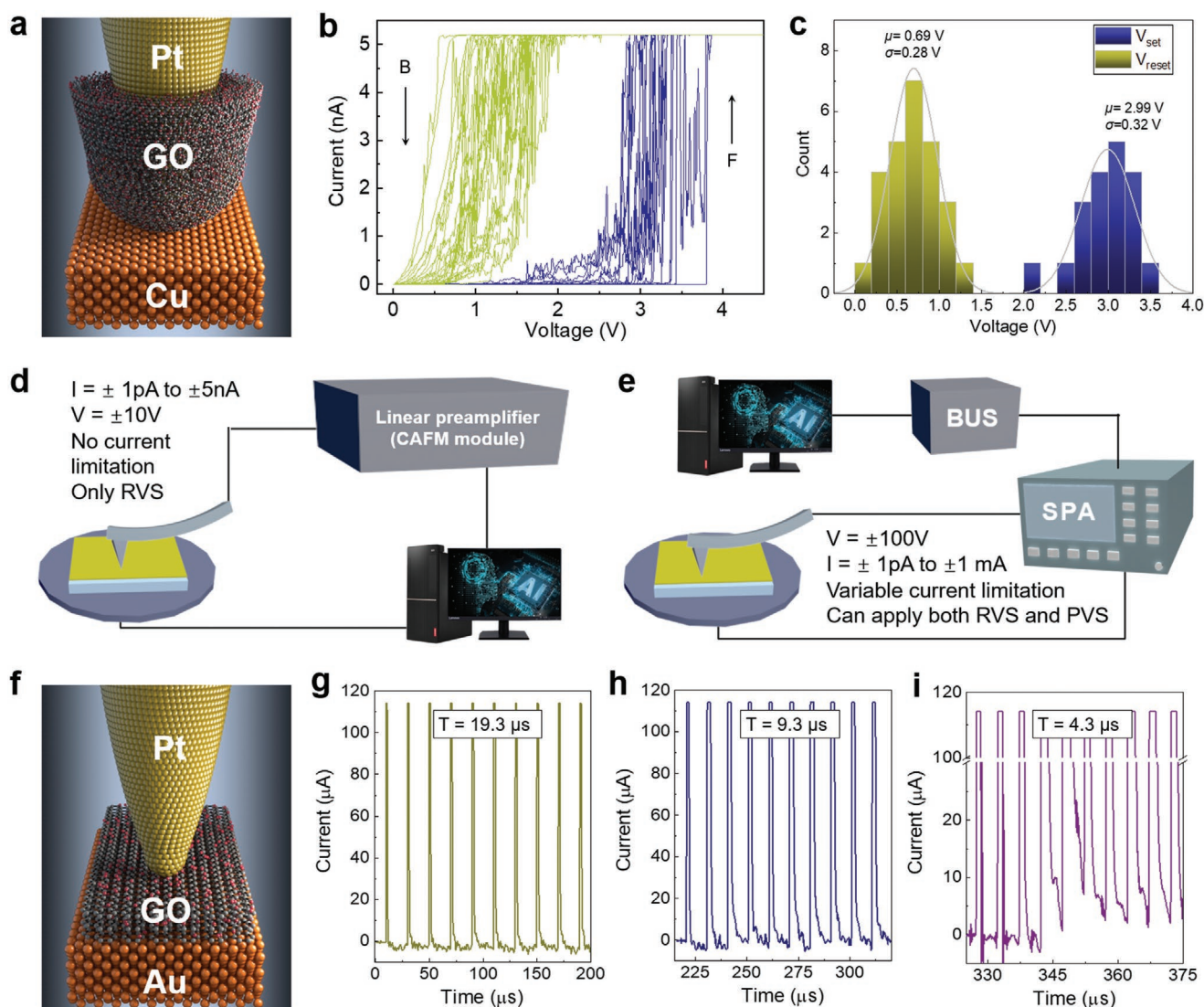


**Figure 2.** Electrical measurement of metal/GO/metal. a) Schematic GO-coated Pt tip on Cu, forming a Pt/GO/Cu nano-synapse with area  $<50 \text{ nm}^2$ . b)  $I$ - $V$  sweeps in a Pt/GO/Cu nano-synapse showing volatile RS. c) Statistical analysis of the switching voltages of Pt/GO/Cu nano-synapse. d,e) Schematic diagrams of standard CAFM and a CAFM connected to a SPA, respectively. f) Schematic of a Pt tip on GO/Au/SiO<sub>2</sub>, forming a Pt/GO/Au nano-synapse with area  $<50 \text{ nm}^2$ . g-i) Current signal driven by a Pt/GO/Au nano-synapse when applying PVS with common width ( $W = 500 \text{ ns}$ ) and amplitude ( $V_{\text{PULSE}} = 2.5 \text{ V}$ ), and  $T = 19.3, 9.3, 4.3 \mu\text{s}$ , respectively.

the currents during the backward  $I$ - $V$  curve vanish at low voltages ( $V_{TIP} < 0.5$  V), and that the next forward  $I$ - $V$  curve exhibits similar currents to the previous forward one, indicate that the RS phenomenon is volatile. The variability from one cycle to another, evaluated through the mean value ( $\mu$ ) and standard deviation ( $\sigma$ ) of the switching voltages,<sup>[28]</sup> is low ( $2.99 \pm 0.32$  V for  $V_{SET}$  and  $0.69 \pm 0.28$  V for  $V_{RESET}$ ), as shown in Figure 2c, and comparable to that of TMO-based memristors,<sup>[29]</sup> indicating the good reproducibility and reliability of the threshold RS behavior. We observed similar threshold RS characteristics for Pt/GO/Au synapses (see Figure S3, Supporting Information).

To have dynamic information about the switching processes (i.e., set and reset) we apply PVS to the metal/GO/metal nano-synapses by connecting a SPA to the tip of the CAFM (see schematic in Figure 2e). When applying fast (<500 ns) PVS, we present the data for the Pt/GO/Au nano-synapses (Figure 2f), because the dynamic current signals are more stable and reproducible than for the Pt/GO/Cu ones. We apply PVS with a pulse width ( $W$ )  $\approx 500$  ns,  $V_{TIP}$  ranging from  $\approx 2.5$  V ( $V_{PULSE}$ ) to 0 V ( $V_{READ}$ ), and different interval times ( $T$ )  $\approx 19.3, 9.3, 4.3$   $\mu$ s (Figure 2g-i). Our experiments indicate that when longer  $T \approx 19.3$   $\mu$ s is used (Figure 2g), the currents flowing across the

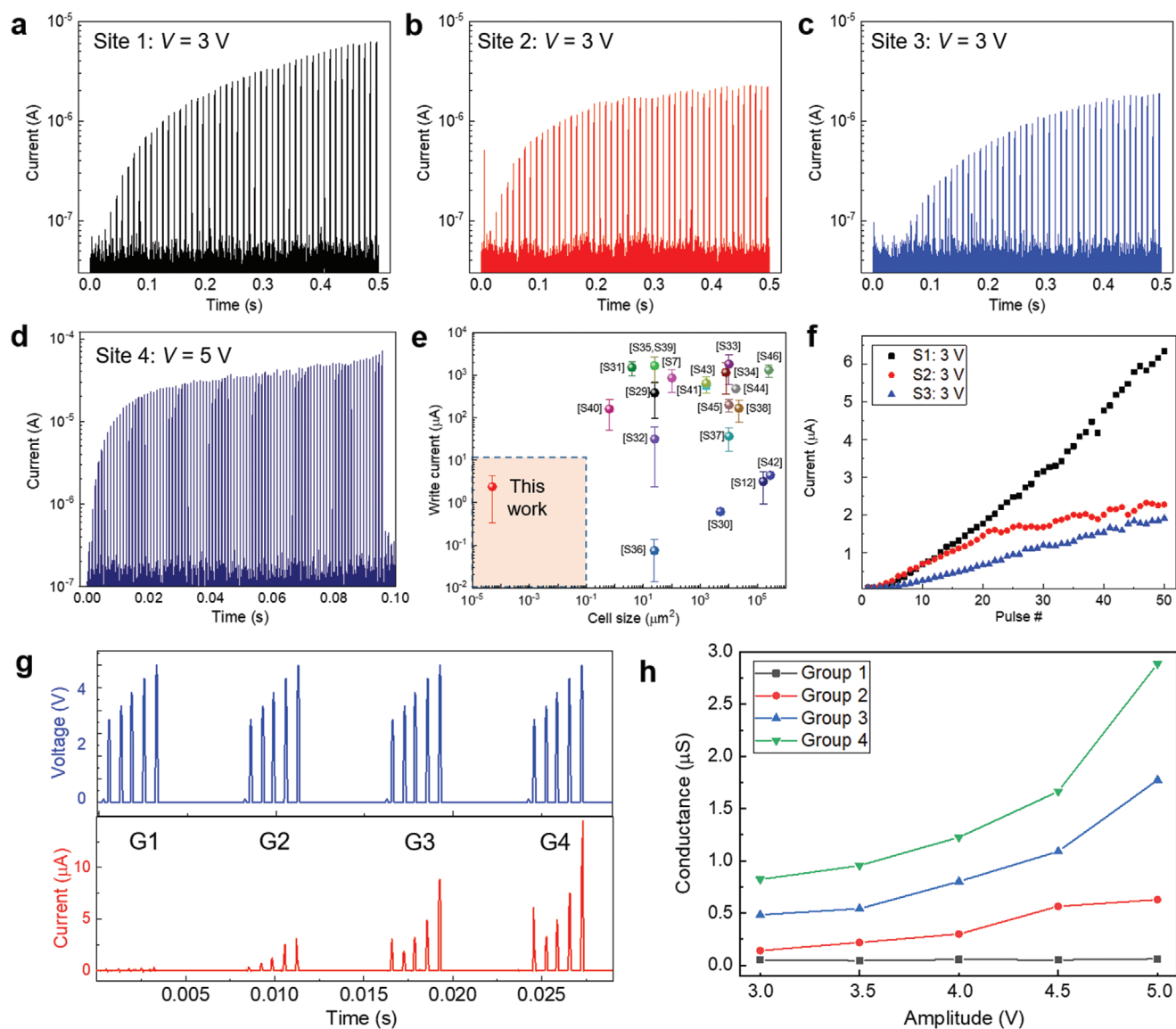


**Figure 3.** Writing current and EPSC in Pt/GO/Au nano-synapses. a–c) Current signals driven by three Pt/GO/Au nano-synapses when applying PVS with common  $W = 1$  ms,  $T = 2$  ms, and  $V_{PULSE} = 3$  V. d) Current signals driven by Pt/GO/Au nano-synapses when applying PVS with common  $W = 100$   $\mu$ s,  $T = 1$  ms, and  $V_{PULSE} = 5$  V. e) Writing current versus cell size for 20 memristive synapses reported in literature and this work. Refs. S7, S12, and S29–S46 are listed in the Supporting Information (see also Table S3, Supporting Information). The orange region outlines the values closer to the technological requirements, as defined in ref. [37]. f) Writing current versus pulse number for the plots in (a–c) showing that potentiation takes place in a linear manner at low currents  $< 1$   $\mu$ A. g) EPSC response (bottom) in one Pt/GO/Au nano-synapse when applying four groups of PVS (G1–G4), each with amplitudes of 3, 3.5, 4, 4.5, 5 V (top). h) Average conductance change in the Pt/GO/Au nano-synapse for PVS of different amplitude, when repeating the experiment in (g) four times in the same synapse.

Pt/GO/Au nano-synapses can complete its relaxation (back to initial current level) after each pulse. On the contrary, when applying shorter  $T \approx 4.3 \mu\text{s}$  (Figure 2i), the currents relaxation is incomplete, and the Pt/GO/Au nano-synapses are erratically potentiated.

By adjusting the width and interval of the PVS ( $W \approx 100 \mu\text{s}$  and  $T \approx 100 \mu\text{s}$ ), analogue potentiation and PPF at wide current ranging from  $\approx 40 \text{ nA}$  to  $\approx 100 \mu\text{A}$  is achieved when applying different pulse amplitudes ( $V_{\text{PULSE}} = 3, 5 \text{ V}$  and  $V_{\text{READ}} = 0 \text{ V}$ ), as shown in **Figure 3a–d**. The speed of the potentiation can be adjusted by tuning the pulse amplitude, and the current across different Pt/GO/Au nano-synapses is similar, indicating that the device-to-device variability is low. The observation of reproducible analogical potentiation at low currents ( $<1 \mu\text{A}$ ) across ultrasmall areas  $<50 \text{ nm}^2$  represents a significant advance in terms of write current and integration density compared to previous literature (see **Figure 3e**). Here, we have the lowest current during the write pulse (not read one) because the read currents are below the intrinsic noise of the SPA operated in pulse mode (i.e.,  $\approx 1 \mu\text{A}$ ), therefore they cannot be measured with this setup. The median power consumption in a potentiation cycle ( $P_{\text{MEDIAN}}$ ), defined as the amplitude of the pulse ( $V_{\text{PULSE}}$ ) multiplied by the median current during the cycle ( $I_{\text{MEDIAN}}$ ), is  $3 \mu\text{W}$ , one of the lowest to date (see **Table S3**, Supporting Information). At such current levels, the potentiation happens in a linear manner (**Figure 3f**), which is also a desired feature in electronic synapses for ANNs.<sup>[30]</sup> The factor  $\approx 2$  variability of the currents between different metal/GO/metal synapses is small compared to state-of-the-art memristors, in which currents fluctuations range from  $5^{[31]}$  to  $1000^{[29]}$  from one device to another. Pt/GO/Au nano-synapses also exhibit EPSC response, i.e., transmission of spikes or action potentials from the presynaptic (Pt) to the post-synaptic neuron (Au) across the GO synapse. **Figure 3g** shows four groups of presynaptic pulses with amplitudes of 3, 3.5, 4, 4.5, 5 V and  $T = 100 \mu\text{s}$  applied to the bulk Pt tip. The EPSC increases with both amplitude and number of presynaptic pulses, **Figure 3g**. This type of EPSC response is similar to that observed in biological excitatory synapses.<sup>[32]</sup> Corresponding excitatory responses (peak values) in each pulse (**Figure 3h**) indicate that the conductance of the Pt/GO/Au nano-synapses starts to increase from the second group, and exhibits an overall increasing trend with the number of groups (upward/downward instabilities from one pulse to another have been observed, normal and similar to those in multiple other studies,<sup>[33–36]</sup> although the overall trend is increasing with the number of groups). There is a conductance decrease after one group with a stop time of 4 ms, indicating a relaxation process of the nano-synapses.

When the polarity of the PVS is inverted (i.e.,  $V_{\text{PULSE}} = -4 \text{ V}$ , with  $T = 100 \mu\text{s}$  and  $W = 100 \mu\text{s}$ ), the Pt/GO/Au nano-synapses exhibit non-volatile conductance increase under long (2000) sequences of PVS up, **Figure 4a**. When the bias is switched-off the conductance does not recover its initial value. The conductance of the Pt/GO/Au nano-synapses can then be decreased by applying PVS with opposed polarity (i.e.,  $V_{\text{PULSE}} = 4 \text{ V}$ ). This is seen in **Figure 4a**, which shows the variability of the currents registered in each conductance state (each box includes 200 data points). These electrical measurements reveal that Pt/GO/Au nano-synapses exhibit stable long-term potentiation and depression, necessary to implement LTP.<sup>[13,38]</sup>

The goal of SPM-based investigations in the field of RS is to demonstrate that the nano-synaptic response can be observed in small areas  $<50 \text{ nm}^2$ , and to describe the quality of the RS phenomenon (i.e., shape of the electrical plots). Multiple studies have considered the switching mechanism in metal/GO/metal memristors by interpreting electrical signals<sup>[21–23]</sup> and chemical techniques with low ( $>5 \mu\text{m}$ ) lateral resolution.<sup>[22,39]</sup> While these are not the recommended methods to study the RS mechanism (only chemical tools with nanoscale lateral resolution or first principles calculations are),<sup>[40]</sup> they can provide some insights. Using a similar approach, our electrical measurements in **Figures 2–4** allow us to make reasonable suggestions. First, the fact that the threshold (i.e., volatile) RS (**Figures 2–3**) is only observed when the potentiation is realized by applying positive voltage to the Pt electrode (see **Figure S4a**, Supporting Information) indicates that this behavior is related to the formation of oxygen vacancies in the GO film. Under these biasing conditions: i) the  $\text{O}^{2-}$  ions, which have a low ( $<0.7 \text{ eV}$ ) activation energy,<sup>[41]</sup> try to move toward the Pt electrode; ii) the  $\text{Pt}^+$  ions, which have a high ( $>0.7 \text{ eV}$ ) activation energy,<sup>[42]</sup> are not able to move; and iii) the  $\text{Cu}^+$  ions (in Pt/GO/Cu devices) and  $\text{Au}^+$  ions (in Pt/GO/Au devices) are pushed away from the GO film. Therefore, the most probable atomic rearrangement is the movement of  $\text{O}^{2-}$  ions (including the transformation between insulating  $\text{sp}^3$  and conducting  $\text{sp}^2$ ), which should result in a local increase of conductance.<sup>[26,43]</sup> The fact that the non-volatile RS is only observed when the potentiation is realized by applying a negative voltage to the Pt electrode (see **Figure S4b**, Supporting Information) points to this being generated by the penetration of metal into the GO film, i.e.,  $\text{Cu}^+$  ions in Pt/GO/Cu and  $\text{Au}^+$  ions in Pt/GO/Au. Under these biasing conditions: i) the  $\text{O}^{2-}$  ions, which have a low activation energy,<sup>[41]</sup> try to move towards the Cu or Au electrode; ii) the  $\text{Pt}^+$  ions, which have a high activation energy,<sup>[42]</sup> are not able to move; and iii) the  $\text{Cu}^+$  ions (in Pt/GO/Cu devices) and  $\text{Au}^+$  ions (in Pt/GO/Au devices), whose diffusivity is  $\approx 3\text{--}4$  times higher than that of Pt,<sup>[44]</sup> can penetrate in the GO film. Therefore, switching is enabled by a combination of movement of  $\text{O}^{2-}$  ions toward the Cu or Au electrode, plus penetration of  $\text{Cu}^+$  or  $\text{Au}^+$  ions in the GO film, as observed in many other devices with similar structure and electrodes.<sup>[44]</sup> Furthermore, our GO film is prepared LPE, which results in defects at the junctions between flakes,<sup>[45]</sup> favoring reversible ion migration at those sites at lower electrical fields.

In order to further understand the conduction across the metal/GO/metal nano-synapses, we carry out additional experiments and calculations. The maximum conductance of the Pt/GO/Au nano-synapses during the potentiation and depression cycles is  $\approx 1.5 \mu\text{S}$ , **Figure 4a**, well below the quantum conductance,  $G_0 = 77.5 \mu\text{S}$ .<sup>[46]</sup> This indicates that RS is driven by the accumulation of defects inside the dielectric, without forming a conductive nanofilament (CNF) across the GO film. In order to validate this, the width of the pulses is increased (i.e.,  $T = 20 \text{ ms}$  and  $W = 10 \text{ ms}$ ). When the conductance of the Pt/GO/Au nano-synapse surpasses  $G_0$  the depression becomes sharper (see **Figure 4b**). This is related to the rupture of a CNF at the transition to sub- $G_0$  conductance. The RS non-volatility when potentiating the Pt/GO/Au nano-synapses by applying a negative voltage to the Pt electrode is confirmed via RVS,

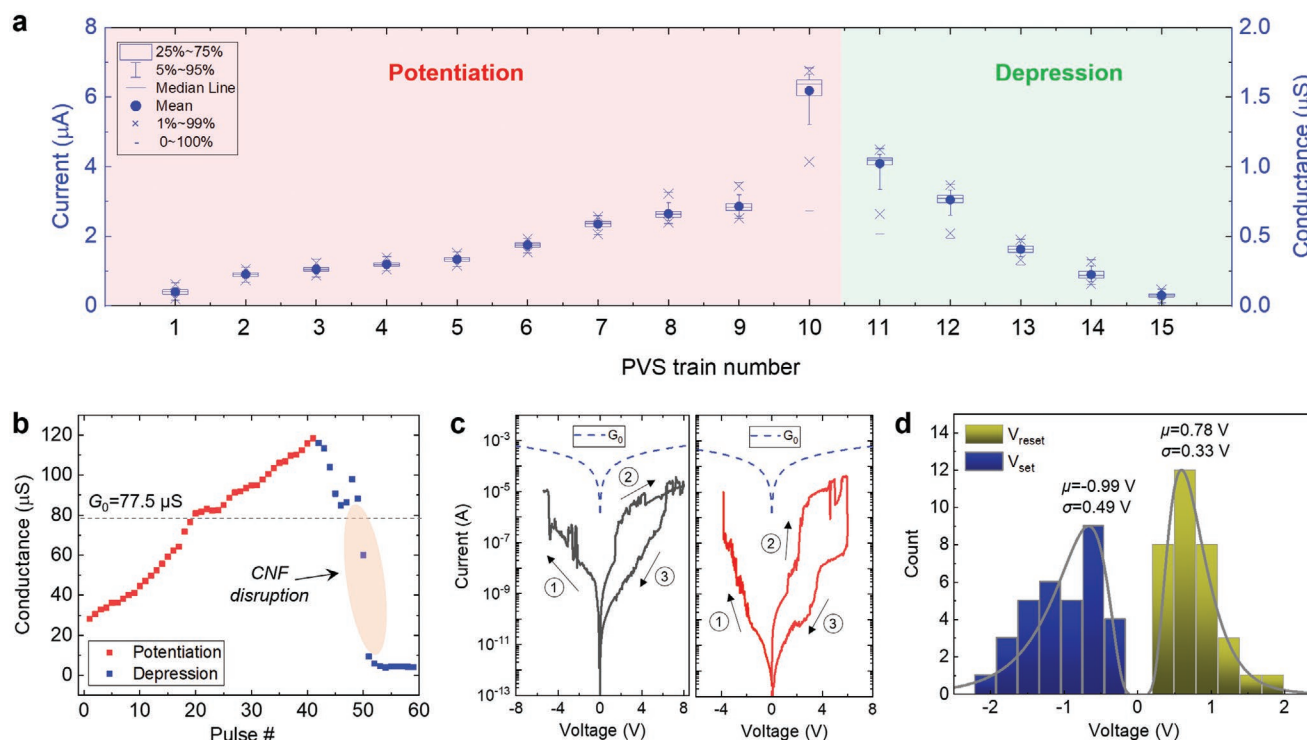


**Figure 4.** Non-volatile RS in Pt/GO/Au nano-synapses. a) Current driven by a Pt/GO/Au nano-synapse when applying PVS trains with  $V_{\text{PULSE}} = -4$  V (potentiation, trains 1–10) and  $V_{\text{PULSE}} = 4$  V (depression, trains 11–15) to the Pt electrode ( $W = 100$   $\mu\text{s}$ ,  $T = 100$   $\mu\text{s}$ ). The value of the conductance is also indicated. b) Conductance of a Pt/GO/Au nano-synapse when applying PVS, showing that above  $G_0$  the disruption is sharp, indicating that a filament was formed and disrupted. c)  $I$ - $V$  characteristics collected in two Pt/GO/Au nano-synapses, showing non-volatile bipolar RS below  $G_0$ , with  $V_{\text{SET}} \approx -4$  V and  $V_{\text{RESET}} \approx 5.5$  V d) Statistical analysis of  $V_{\text{SET}}$  and  $V_{\text{RESET}}$  for a Pt/GO/Cu nano-synapse, showing that the switching voltage when using Cu electrodes is lower than when using Au electrodes.

which exhibit  $V_{\text{SET}} \approx -4$  V and  $V_{\text{RESET}} \approx 5.5$  V (see Figure 4c,d). The switching voltages can be further decreased when using Cu as electrode (instead Au), as it has a higher diffusivity.<sup>[47]</sup> Figure 4e shows that Pt/GO/Cu nano-synapses exhibit non-volatile bipolar RS with  $V_{\text{SET}} \approx 0.99$  V and  $V_{\text{RESET}} \approx 0.78$  V. The variability of  $V_{\text{SET}}$  and  $V_{\text{RESET}}$  from one cycle to the other is consistent with that observed in other RS devices,<sup>[38]</sup> and does not represent a problem for their use as electronic synapse in ANNs.<sup>[40]</sup> The fact that bipolar RS is observed at conductance  $<G_0$  (Figure 4c,d) also indicates that no CNF is completely formed across the GO film. We calculate the relative temperature increase in the metal/GO/metal nano-synapses during the  $I$ - $V$  curves in Figure 4c, using the model of ref. [48], as it follows the heat equation presented in Note S2, Supporting Information. Our calculations (see Note S2, Supporting Information) indicate that, at those current regimes, thermal effects are negligible. The temperature increase for the maximum current  $\approx 30$   $\mu\text{A}$  (at  $\approx 6$  V) is  $<320$  K. This observation further points to ionic migration being responsible for RS, and to the fact that no CNF is formed in either volatile (Figures 2 and 3) and non-volatile (Figure 4a) regimes.

### 3. Conclusion

In conclusion, we probed the nano-synaptic response in GO films in ultrasmall areas ( $<500$   $\text{nm}^2$ ) by using a CAFM

connected to a SPA. The GO films were deposited on metal-coated wafers and bulk Pt tips using an industry-compatible spray-coating methodology, achieving conformal coating. The metal/GO/metal nano-synapses emulate potentiation and PPF at low current levels  $<1$   $\mu\text{A}$ , controllable EPSC and controllable long-term potentiation and depression, and non-volatile bipolar RS (necessary to emulate LTP) at higher current ranges. Both RS mechanisms take place at very low operating currents (i.e., conductance  $<G_0$ , i.e., non-filamentary mechanism), resulting in a very low power consumption ( $\approx 3$   $\mu\text{W}$ ). Our work provides a route to detect nano-synaptic responses in different types of materials, and indicates that GO may be an excellent RS medium to fabricate small area ( $<50$   $\text{nm}^2$ ) memristive electronic synapses (operating at low current ranges) for high-density ANNs.

### 4. Experimental Section

**Graphene Oxide Preparation:** GO is prepared as follows. Step 1 - Pretreatment: Graphite flakes (3g, Sigma-Aldrich) are mixed with 98% sulfuric acid ( $\text{H}_2\text{SO}_4$ , 12 mL), potassium persulfate ( $\text{K}_2\text{S}_2\text{O}_8$ , 2.5 g), and phosphorus pentoxide ( $\text{P}_2\text{O}_5$ , 2.5 g) and the mixture is heated to 80  $^\circ\text{C}$  for 5 h. The mixture is then diluted with de-ionized water ( $\text{H}_2\text{O}$ , 0.5 L), filtered, and washed with de-ionized  $\text{H}_2\text{O}$  (thrice) to remove the residual acid. The resultant is dried at 80  $^\circ\text{C}$  overnight. Step 2-Oxidation by Hummers' method:<sup>[49]</sup> The pretreated graphite flakes are transferred into 98%  $\text{H}_2\text{SO}_4$  (120 mL) cooled in an ice bath. Then, potassium

permanganate (KMnO<sub>4</sub>, 15 g) is added gradually under stirring to keep the temperature <20 °C. The mixture is stirred at 35 °C for 4 h, and diluted with de-ionized (DI) H<sub>2</sub>O (250 mL). Afterwards the mixture is stirred for 2 h at 90 °C, followed by the addition of DI H<sub>2</sub>O (0.7 L). Hydrogen peroxide (H<sub>2</sub>O<sub>2</sub>, 30%, 20 mL) is then added, and the resulting brilliant-yellow mixture is filtered and washed with hydrochloric acid aqueous solution (HCl, 10 wt%) to remove metal ions. GO is then washed repeatedly in order to remove residual acid with H<sub>2</sub>O until neutral pH and then diluted to yield a GO dispersion with concentration ≈5 g L<sup>-1</sup>. Immediately before spray coating, the GO is diluted with ethanol to a give a final concentration ≈0.5 g L<sup>-1</sup>. After the preparation of GO, the flakes are dispersed in ethanol at a concentration ≈0.5 mg mL<sup>-1</sup> to make the GO ink.

**Spray Coating:** An air-assist atomizer (Specialty Coating Systems Precisioncoat V) is used to deposit the GO ink. An array of ten nanopores is positioned ≈8 cm under the spray nozzle. The flow rate is set to 13.5 mL min<sup>-1</sup> to control the speed of liquid ejection from the spray nozzle. An atomization pressure (i.e., the gas pressure applied across the liquid ejected from the spray nozzle) ≈9 psi is used. The nozzle is moved at ≈12.7 cm s<sup>-1</sup> across the array of nanopores to cover them with GO ink. The coating process is undertaken at 20 °C to minimize the surface roughness. The spray nozzle is passed over the array of nanopores five times (i.e., five coating layers) to create the GO film. The same conditions are used to coat the SiO<sub>2</sub> wafers.

**Electrical Measurements:** Three CAFM systems are utilized: 1) NX-HighVac from Park Systems, 2) Bruker Dimension Icon from Bruker, and 3) Multimode V from Veeco. All equipped with Pt tips from Rocky Mountain (model RMN-25PT300B), with a tip radius <8 nm and a nominal spring constant ≈18 N m<sup>-1</sup>. For all CAFM tests, the voltages are applied to the CAFM tip, while keeping the sample substrate grounded. The use of solid bulk Pt is important to ensure high stability (i.e., metal-varnished Si tips degrade easily after some measurements) and make data measurements highly reliable. When measuring PVS or I-V curves with enhanced voltage and current ranges, electrical stresses are applied to the CAFM tip using the SMU1 of a B1500A SPA, and the post-synaptic currents are collected with the SPA SMU2, Figure 2e. The nominal contact force between tip and sample during RVS and PVS is ≈2 nN, in order to avoid GO film deformation. The contact resistance between tip and a metallic sample is ≈10 Ω, negligible compared to the high resistance detected in the metal/GO/metal device due to the insulating nature of the GO film.

## Supporting Information

Supporting Information is available from the Wiley Online Library or from the author.

## Acknowledgements

The authors acknowledge funding by the Ministry of Science and Technology of China (grant no. 2018YFE0100800, 2019YFE0124200), the National Natural Science Foundation of China (grant no. 61874075), the Ministry of Finance of China (grant no. SX21400213), the Jiangsu Planned Projects for Postdoctoral Research Funds of China (grant No. 7131712019), the 111 Project from the State Administration of Foreign Experts Affairs of China, the Collaborative Innovation Centre of Suzhou Nano Science & Technology, the Jiangsu Key Laboratory for Carbon-Based Functional Materials & Devices, the Priority Academic Program Development of Jiangsu Higher Education Institutions, the Isaac Newton Trust, the EU project CareRAMM, EU Graphene Flagship, ERC grants Hetero2D and MINERGRACE, EPSRC grants EP/K01711X/1, EP/K017144/1, EP/N010345/1, EP/M507799/1, EP/L016087/1, EP/R511547/1, EP/P02534X/2, EP/T005106/1, and a Technion-Guangdong Fellowship.

## Conflict of Interest

The authors declare no conflict of interest.

## Data Availability Statement

Research data are not shared.

## Keywords

conductive atomic force microscopy, electronic synapses, graphene oxide, resistive switching, spray coating, synaptic plasticity

Received: February 24, 2021

Revised: March 27, 2021

Published online: June 3, 2021

- [1] D. Ielmini, R. Waser, *Resistive Switching: From Fundamentals of Nanoionic Redox Processes to Memristive Device Applications*, Wiley-VCH, Germany **2016**.
- [2] A. Chen, S. Haddad, Y.-C. Wu, T.-N. Fang, Z. Lan, S. Avanzino, S. Pangrle, M. Buynoski, M. Rathor, W. Cai, N. Tripsas, C. Bill, M. Van Buskirk, M. Taguchi, in *IEEE Int. Electron Devices Meeting, 2005. IEDM Technical Digest*, IEEE, Washington, DC **2005**.
- [3] K. D. M. Rao, A. A. Sagade, R. John, T. Pradeep, G. U. Kulkarni, *Adv. Electron. Mater.* **2016**, *2*, 1500286.
- [4] Q. Xia, J. J. Yang, *Nat. Mater.* **2019**, *18*, 309.
- [5] J. J. Yang, M. D. Pickett, X. Li, D. A. A. Ohlberg, D. R. Stewart, R. S. Williams, *Nat. Nanotechnol.* **2008**, *3*, 429.
- [6] S. Pi, C. Li, H. Jiang, W. Xia, H. Xin, J. J. Yang, Q. Xia, *Nat. Nanotechnol.* **2019**, *14*, 35.
- [7] B. Govoreanu, G. S. Kar, Y.-Y. Chen, V. Paraschiv, S. Kubicek, A. Fantini, I. P. Radu, L. Goux, S. Clima, R. Degraeve, N. Jossart, O. Richard, T. Vandeweyer, K. Seo, P. Hendrickx, G. Pourtois, H. Bender, L. Altimime, D. J. Wouters, J. A. Kittl, M. Jurczak, in *2017 Int. Electron Devices Meeting*, IEEE, Washington, DC **2017**.
- [8] M. Lanza, M. Porti, M. Nafria, X. Aymerich, G. Benstetter, E. Lodermeier, H. Ranzinger, G. Jaschke, S. Teichert, L. Wilde, P. Michalowski, *Microelectron. Eng.* **2009**, *86*, 1921.
- [9] W. Frammelsberger, G. Benstetter, J. Kiely, R. Stamp, *Appl. Surf. Sci.* **2007**, *253*, 3615.
- [10] A. Nayak, T. Ohno, T. Tsuruoka, K. Terabe, T. Hasegawa, J. K. Gimzewski, M. Aono, *Adv. Funct. Mater.* **2012**, *22*, 3606.
- [11] T. Ohno, T. Hasegawa, T. Tsuruoka, K. Terabe, J. K. Gimzewski, M. Aono, *Nat. Mater.* **2011**, *10*, 591.
- [12] R. S. Zucker, *Annu. Rev. Neurosci.* **1989**, *12*, 13.
- [13] A. Hyvarinen, in *NIPS Proceedings*, (Eds: M. Jordan, M. Kearns, S.olla), MIT Press, Cambridge, MA **1997**, pp. 273–279.
- [14] M. Lanza, *Conductive Atomic Force Microscopy: Application in Nanomaterials*, Wiley-VCH, Weinheim **2017**.
- [15] Y. Hernandez, V. Nicolosi, M. Lotya, F. M. Blighe, Z. Sun, S. De, I. T. McGovern, B. Holland, M. Byrne, Y. K. Gun'ko, J. J. Boland, P. Niraj, G. Duesberg, S. Krishnamurthy, R. Goodhue, J. Hutchison, V. Scardaci, A. C. Ferrari, J. N. Coleman, *Nat. Nanotechnol.* **2008**, *3*, 563.
- [16] F. Hui, M. Lanza, *Nat. Electron.* **2019**, *2*, 221.
- [17] V. Iglesias, X. Jing, M. Lanza, in *Conductive Atomic Force Microscopy: Application in Nanomaterials* (Ed. M. Lanza), Wiley-VCH, Weinheim **2017**, Ch. 10.
- [18] F. Hui, E. Grustan-Gutierrez, S. Long, Q. Liu, A. K. Ott, A. C. Ferrari, M. Lanza, *Adv. Electron. Mater.* **2017**, *3*, 1600195.

- [19] A. K. Ott, C. Dou, U. Sassi, I. Goykhman, D. Yoon, J. Wu, A. Lombardo, A. C. Ferrari, *2D Mater.* **2018**, *5*, 045028.
- [20] T. Ahmed, S. Kuriakose, E. L. H. Mayes, R. Ramanathan, V. Bansal, M. Bhaskaran, S. Sriram, S. Walia, *Small* **2019**, *15*, 1900966.
- [21] Y. Yang, J. Wen, L. Guo, X. Wan, P. Du, P. Feng, Y. Shi, Q. Wan, *ACS Appl. Mater. Interfaces* **2016**, *8*, 30281.
- [22] A. S. Sokolov, M. Ali, R. Riaz, Y. Abbas, M. J. Ko, C. Choi, *Adv. Funct. Mater.* **2019**, *29*, 1807504.
- [23] Y. Park, M.-J. Park, J.-S. Lee, *Adv. Funct. Mater.* **2018**, *28*, 1804123.
- [24] A. F. M. Ibrahim, Y. S. Lin, *Chem. Eng. Sci.* **2018**, *190*, 312.
- [25] C. Backes, A. M. Abdelkader, C. Alonso, A. Andrieux-Ledier, R. Arenal, J. Azpeitia, N. Balakrishnan, L. Banszerus, J. Barjon, R. Bartali, S. Bellani, C. Berger, R. Berger, M. M. B. Ortega, C. Bernard, P. H. Beton, A. Beyer, A. Bianco, P. Bøggild, F. Bonaccorso, G. B. Barin, C. Botas, R. A. Bueno, D. Carriazo, A. Castellanos-Gomez, M. Christian, A. Ciesielski, T. Ciuk, M. T. Cole, J. Coleman, C. Coletti, L. Crema, H. Cun, D. Dasler, D. De Fazio, N. Diez, S. Drieschner, G. S. Duesberg, R. Fasel, X. Feng, A. Fina, S. Forti, C. Galiotis, G. Garberoglio, J. M. García, J. A. Garrido, M. Gibertini, A. Götzhäuser, J. Gómez, T. Greber, F. Hauke, A. Hemmi, I. Hernandez-Rodriguez, A. Hirsch, S. A. Hodge, Y. Huttel, P. U. Jepsen, I. Jimenez, U. Kaiser, T. Kaplas, H. Kim, A. Kis, K. Papagelis, K. Kostarelos, A. Krajewska, K. Lee, C. Li, H. Lipsanen, A. Liscio, M. R. Lohe, A. Loiseau, L. Lombardi, M. F. López, O. Martin, C. Martín, L. Martínez, J. A. Martin-Gago, J. I. Martínez, N. Marzari, Á. Mayoral, J. Mcmanus, M. Melucci, J. Méndez, C. Merino, P. Merino, A. P. Meyer, E. Miniussi, V. Miseikis, N. Mishra, V. Morandi, C. Munuera, R. Muñoz, H. Nolan, L. Ortolani, A. K. Ott, I. Palacio, V. Palermo, J. Parthenios, I. Pasternak, A. Patane, M. Prato, H. Prevost, V. Prudkovskiy, N. Pugno, T. Rojo, A. Rossi, P. Ruffieux, P. Samori, L. Schué, E. Setijadi, T. Seyller, G. Speranza, C. Stampfer, I. Stenger, W. Strupinski, Y. Svirko, S. Taioli, K. B. K. Teo, M. Testi, F. Tomarchio, M. Tortello, E. Treossi, A. Turchanin, E. Vazquez, E. Villaro, P. R. Whelan, Z. Xia, R. Yakimova, S. Yang, G. R. Yazdi, C. Yim, D. Yoon, X. Zhang, X. Zhuang, L. Colombo, A. C. Ferrari, M. Garcia-Hernandez, *2D Mater.* **2020**, *7*, 022001.
- [26] Romero, Toral-Lopez, Ohata, Morales, Ruiz, Godoy, Rodriguez, *Nanomaterials* **2019**, *9*, 897.
- [27] F. Torrisi, T. Carey, *Nano Today* **2018**, *23*, 73.
- [28] G. C. Adam, B. D. Hoskins, M. Prezioso, F. Merrikh-Bayat, B. Chakrabarti, D. B. Strukov, *IEEE Trans. Electron Devices* **2017**, *64*, 312.
- [29] A. Fantini, L. Goux, A. Redolfi, R. Degraeve, G. Kar, Y. Y. Chen, M. Jurczak, in *2014 Symp. on VLSI Technology (VLSI-Technology): Digest of Technical Papers*, IEEE, Honolulu, HI **2014**.
- [30] W. Zhang, B. Gao, J. Tang, X. Li, W. Wu, H. Qian, H. Wu, *Phys. Status Solidi RRL* **2019**, *13*, 1900204.
- [31] S. Chen, M. R. Mahmoodi, Y. Shi, C. Mahata, B. Yuan, X. Liang, C. Wen, F. Hui, D. Akinwande, D. B. Strukov, M. Lanza, *Nat. Electron.* **2020**, *3*, 638.
- [32] W. Xu, S.-Y. Min, H. Hwang, T.-W. Lee, *Sci. Adv.* **2016**, *2*, e1501326.
- [33] Z. Wang, S. Joshi, S. E. Savel'ev, H. Jiang, R. Midya, P. Lin, M. Hu, N. Ge, J. P. Strachan, Z. Li, Q. Wu, M. Barnell, G.-L. Li, H. L. Xin, R. S. Williams, Q. Xia, J. J. Yang, *Nat. Mater.* **2017**, *16*, 101.
- [34] S. H. Jo, T. Chang, I. Ebong, B. B. Bhadviya, P. Mazumder, W. Lu, *Nano Lett.* **2010**, *10*, 1297.
- [35] S. Kim, H. Kim, S. Hwang, M.-H. Kim, Y.-F. Chang, B.-G. Park, *ACS Appl. Mater. Interfaces* **2017**, *9*, 40420.
- [36] X. Yan, J. Zhao, S. Liu, Z. Zhou, Q. Liu, J. Chen, X. Y. Liu, *Adv. Funct. Mater.* **2018**, *28*, 1705320.
- [37] International Technology Roadmap for Semiconductors, 2013 Edition, Process Integration, Devices, and Structures Section, <https://www.semiconductors.org/resources/2013-international-technology-roadmap-for-semiconductors-itrs/> (accessed: February 2015).
- [38] Y. Shi, X. Liang, B. Yuan, V. Chen, H. Li, F. Hui, Z. Yu, F. Yuan, E. Pop, H.-S. P. Wong, M. Lanza, *Nat. Electron.* **2018**, *1*, 458.
- [39] Website of Thermo Fisher Scientific, [www.thermofisher.com/](http://www.thermofisher.com/) (accessed: March 2021).
- [40] M. Lanza, H.-S. P. Wong, E. Pop, D. Ielmini, D. Strukov, B. C. Regan, L. Larcher, M. A. Villena, J. J. Yang, L. Goux, A. Belmonte, Y. Yang, F. M. Puglisi, J. Kang, B. Magyari-Köpe, E. Yalon, A. Kenyon, M. Buckwell, A. Mehonic, A. Shluger, H. Li, T.-H. Hou, B. Hudec, D. Akinwande, R. Ge, S. Ambrogio, J. B. Roldan, E. Miranda, J. Suñe, K. L. Pey, X. Wu, N. Raghavan, E. Wu, W. D. Lu, G. Navarro, W. Zhang, H. Wu, R. Li, A. Holleitner, U. Wurstbauer, M. C. Lemme, M. Liu, S. Long, Q. Liu, H. Lv, A. Padovani, P. Pavan, I. Valov, X. Jing, T. Han, K. Zhu, S. Chen, F. Hui, Y. Shi, *Adv. Electron. Mater.* **2018**, *5*, 1800143.
- [41] O. Pirrotta, A. Padovani, L. Larcher, L. Zhao, B. Magyari-Köpe, Y. Nishi, in *2014 Int. Conf. on Simulation of Semiconductor Processes and Devices (SISPAD)IEEE, Piscataway, NJ* **2014**.
- [42] Y. Yang, P. Gao, S. Gaba, T. Chang, X. Pan, W. Lu, *Nat. Commun.* **2012**, *3*, 732.
- [43] S. Porro, E. Accornero, C. F. Pirri, C. Ricciardi, *Carbon* **2015**, *85*, 383.
- [44] F. Zhuge, B. Hu, C. He, X. Zhou, Z. Liu, R.-W. Li, *Carbon* **2011**, *49*, 3796.
- [45] X. Jing, Y. Illarionov, E. Yalon, P. Zhou, T. Grasser, Y. Shi, M. Lanza, *Adv. Funct. Mater.* **2020**, *30*, 1901971.
- [46] C. Pan, E. Miranda, M. A. Villena, N. Xiao, X. Jing, X. Xie, T. Wu, F. Hui, Y. Shi, M. Lanza, *2D Mater.* **2017**, *4*, 025099.
- [47] Y. Yang, P. Gao, L. Li, X. Pan, S. Tappertzhofen, S. Choi, R. Waser, I. Valov, W. D. Lu, *Nat. Commun.* **2014**, *5*, 4232.
- [48] M. Maestro-Izquierdo, M. B. Gonzalez, F. Jimenez-Molinos, E. Moreno, J. B. Roldan, F. Campabadal, *Nanotechnology* **2020**, *31*, 135202.
- [49] W. S. Hummers, R. E. Offeman, *J. Am. Chem. Soc.* **1958**, *80*, 1339.